Ocean Engineering 310 (2024) 118648

Contents lists available at ScienceDirect

Ocean Engineering

journal homepage: www.elsevier.com/locate/oceaneng

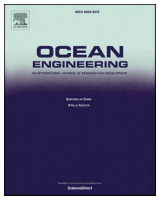

Research paper

Prediction of waves in tanks excited by ship motion and moving walls with a three-dimensional fully linear finite difference approach

Yan Qi [a,*], Heinrich Söding [c], Jasmin Stöcker [a], Marcel Zydeck [b], Jens Neugebauer [a], Ould el Moctar [a], Thomas E. Schellin [a]

[a] University of Duisburg-Essen - Institute of Ship Technology, Ocean Engineering and Transport Systems, Duisburg, North Rhine-Westphalia, Germany
[b] University of Duisburg-Essen - Chair of Dynamics and Control, Duisburg, North Rhine-Westphalia, Germany
[c] Hamburg University of Technology-Institute of Fluid Dynamics and Ship Theory, Hamburg, Germany

ARTICLE INFO

Keywords:
Sloshing
Navier-Stokes equations
Volume-of-fluid method
Overset technique
Finite difference method
Frequency domain
Wave damping
Model test

ABSTRACT

Mitigation of waves in shipboard swimming pools excited by ship motions is a topic of current interest that has not yet been extensively investigated. Various damping mechanisms have been applied to mitigate waves excited in tanks, such as porous baffles or different types of internal baffles. However, most of these devices are installed in LNG tanks to prevent serious sloshing effects. Furthermore, these are passive devices and, hence, unable to control wave-induced excitations. Our focus was on the validation and verification of the three-dimensional (3D) fully linear Finite Difference Method (FDM) based on the previously developed method of Qi et al. (2024) for predicting waves in a transversely placed swimming pool excited by ship motions and piston-type actuators. We validated our FDM approach against comparative Computational Fluid Dynamics (CFD) simulations as well as experimental model test measurements. The CFD tools solved the Reynolds-averaged Navier-Stokes (RANS) equations, relied on an appropriate turbulence model and the Volume of Fluid (VOF) method to capture the free surface of the liquid in the model tank, and employed the overset technique to specify the motions of the active actuators. Our FDM considered ship-induced roll excitations as well as simultaneous roll and sway excitations, albeit only at frequencies outside the range of the pool's resonance frequency. For these periods, our approach accurately predicted not only the mitigated waves in the pool, but also the optimum amplitude of the actuators needed to mitigate such waves. Our FDM can be applied to obtain a preview of excited waves under various conditions, leveraging its principal advantage of extreme computational efficiency.

1. Introduction

With the end of the pandemic, the global economy has progressively recovered in recent years, and so did the tourism industry. As a result, the yacht industry began to grow steadily, exemplified by many newly built super yachts equipped with swimming pools. Swimming pools on yachts are conventionally placed longitudinally at their stern or forward areas to prevent the occurrence of waves excited in pools due to the ship's roll and sway motions. On ships are equipped with active antiroll fins, roll motions are significantly reduced. In such cases, swimming pools are often situated transversely. As the ship's natural roll and sway periods are usually designed to be larger than the eigenperiod of waves excited in a shipboard swimming pool, the amplitudes of these waves are small. Therefore, they can be precisely predicted using numerical tools relying on linear mathematical models.

Generation and absorption of waves has been a topic that many researchers investigated for decades. Many concepts and mechanisms based on potential theory have been developed, tested, and validated to make waves in water channels. In general, concepts of wave makers can also be applied to mitigate waves caused by the same mechanism. One of the most common and effective ways to generate waves is using a piston-type wave maker derived from the classical Boussinesq equation. Although many researchers contributed to the development of nonlinear wave maker theories, it was Schäffer (1996) who proposed the second-order wave maker theory for generating irregular waves, and we focused on his theory to generate linear waves in our work. Skourup et al. (1996, 1997) started their numerical study on active mechanisms for wave absorption in wave tanks by applying a Boundary Element

* Corresponding author.
E-mail address: yan.qi@uni-due.de (Y. Qi).

https://doi.org/10.1016/j.oceaneng.2024.118648
Received 25 March 2024; Received in revised form 24 June 2024; Accepted 2 July 2024
Available online 14 July 2024

Method (BEM). Wu et al. (2014, 2016) performed their numerical and experimental study by generating solitary waves in a wave flume using a piston-type wave maker and applying Fenton's solitary solution to the paddle motion. Their research demonstrated the advantageous performance of their technique with wave makers in. By solving the RANS equations in a commercial CFD code together with the VOF method, Prasad et al. (2017) validated a piston-type wave maker using a numerical wave tank. To include shallow water effects and to observe the propagation of low amplitude solitary waves, Park et al. (2023) carried out their investigation on a new kind of piston-type wave maker. A step-type piston wave maker was also investigated analytically and verified, using a higher order BEM, by Zhou et al. (2010). Furthermore, Kim et al. (2021) conducted an analytical study on a multi-paddle piston wave maker and carried out CFD simulations in OpenFOAM. Other types of wave makers were also studied, such as a wedge-shaped plunger wave maker by Sun et al. (2021). These studies demonstrated that a piston-type wave maker is an effective and simple way to generate waves. Hence, here we considered piston-type actuators to demonstrate their feasibility of mitigating waves in a transversely placed swimming pool.

Apparently, the generation and mitigation of waves in water channels differs greatly in swimming pools, where the reflected waves play a relevant roll and where violent sloshing-induced waves may occur. Indeed, various structural or floating mechanisms installed inside partially filled LNG tanks have been investigated to suppress sloshing-induced waves. Using the method of superposition of modes, Gedikli et al. (1999) presented their seismic analysis of a cylindrical liquid storage tank with a baffle. Based on their work, Maleki et al. (2007, 2008) investigated the effectiveness of ring and vertical baffle structures situated in cylindrical tanks by carrying out a series of experiments. Although other researchers contributed further to the investigation of baffles in cylindrical or elliptical tanks experimentally and numerically, for instance, Akyldz et al. (2013), Hasheminejad et al. (2012), and Wang et al. (2023), most efforts on mitigation of waves were made in rectangular or cubic tanks, which are commonly applied and simpler to use to numerically model analytical solutions. Waldie et al. (2000) carried out experiments to study two perforated baffle designs and one solid strip baffle situated in a model vessel. Experiments were also carried out with and without baffles by Panigrahy et al. (2009) to observe the consequential changes under various conditions. By applying a velocity-potential based nonlinear FEM, Cho and Lee (2004) investigated sloshing phenomena in a two-dimensional baffled tank. The Large-Eddy-Simulation (LES) approach of Liu and Lin (2009) yielded accurate predictions of fluid motions in tanks with vertical baffles, and they discussed the effect of baffles. Eswaran et al. (2009) presented their comparative study on the analysis of sloshing waves in baffled and un-baffled tanks using the Arbitrary Lagrangian-Eulerian (ALE) method to demonstrate the effectiveness of baffles.

In the past decades, numerical models were developed and applied to investigate the effectiveness of various types of baffles situated in tanks to enhance the suppression of sloshing waves in tanks. Koh et al. (2013) applied the improved Consistent Particle Method (CPM) to study the effect of a constrained floating baffle by comparing results with experimental measurements. Vertical floating baffles were studied numerically by Bellezi et al. (2022). Sloshing waves in tanks equipped with elastic baffles were investigated by Zhang et al. (2020) numerically, based on the coupling strategy of the Smoothed Finite Element Method (SFEM) and the Smoothed Particle Hydrodynamics (SPH) approach, and they presented the significant effect of elastic baffles on mitigation of sloshing. Cao et al. (2023) proposed their semi-analytical solutions for a two-dimensional (2D) liquid tank with elastic vertical baffles. Dual vertical baffles and multi-layer horizontal baffles were numerically investigated by Jin et al. (2022a, 2022b). Besides, porous baffles gained researcher's attention due to their advantages to reduce turbulence. George and Cho (2021) studied the horizontal porous baffle and its effect as an anti-sloshing device based on an analytical model and experiments. Wang et al. (2022) further carried out their numerical investigation on the damping performance of porous baffles by comparing their results with sloshing experiments. Similar investigations were carried out also by Nimisha et al. (2022), focusing on sloshing-induced damping efficiency. By adding a viscous top-layer fluid, Korkmarz (2022) creatively proposed his concept to dampen sloshing-induced impacts. Recently, angular, and linear spring systems linked to a dual baffle situated in a liquid tank to suppress sloshing phenomena was proposed and evaluated by Saghi et al. (2022), which has been proven to be effective.

As discussed, excited waves in tanks have typically been mitigated using passive mechanisms to minimize sloshing phenomena. In our study, we considered piston-type actuators installed at the ends of swimming pools, moving harmonically at the same period as the ship motion-induced excitations, to actively mitigate excited waves in pools. Investigating such problems involving various periods, amplitudes of actuators, and different water depths in pools results in a significant computational effort when employing CFD tools or other numerical approaches. On the one hand, preparing a calculation using CFD tools, such as designing proper grids that must be well refined near the fluid free surface to capture excited waves accurately, is time-consuming. On the other hand, a 3D CFD calculation that lasts for over 30 excitation periods requires at least several hours, even when carried out on a computational cluster using multiple cores. In contrast, the FDM calculates much more efficiently, with a speed of less than 0.5 s per case on a local computer, significantly improving the efficiency of investigating these issues. Due to the current limitations of the FDM in solving nonlinear waves in pools, we must validate and verify it for periods outside the resonance range, focusing on small amplitudes of excitations and actuators.

In this paper, we specified boundary conditions in the FDM to define control volumes for the actuators situated at the pool's ends, which moved harmonically about their original positions with given amplitudes and at specified frequencies. Our initial focus was on verifying the FDM outside the pool's resonance against comparative results from CFD simulations that solved the RANS equations, incorporating the VOF method and the overset technique. Additionally, we compared our predictions with physical model test measurements conducted in the sloshing lab of the University of Duisburg-Essen. A novel method was used to determine the associated non-dimensional damping parameter, δ. Outside the pool's resonance frequencies, our FDM yielded favorable predictions of excited waves in the pool under the influence of harmonically moving piston-type actuators.

Relying on the extremely fast computation speed of the FDM in the frequency domain, we are able to obtain a preview of excited waves in pools considering piston-type actuators situated at the pool's ends. This capability is particularly valuable and helpful during the design stage of a ship with swimming pools. At the current stage, our approach is not able to accurately solve excited waves in pools at the pool's resonance frequencies. However, it can be applied to preliminarily demonstrate the feasibility of mitigating waves using piston-type actuators for different tank geometries, periods outside the pool's resonance, various water depths, etc. In the final section of the paper, we extended the application of the FDM with an example for predicting the optimum amplitudes of piston-type actuators that most effectively mitigate excited waves in a pool, even near resonance. Further development of the approach is needed to accurately solve nonlinear waves in pools.

2. Numerical approach

2.1. The Finite Difference Method

Although Qi et al. (2024) considered similar cases without moving actuators, we used their mathematical formulations to account for the effect of moving actuators to dampen shallow water waves in a pool excited by ship motions. Assuming that tank motions are small, the fluid

surface does not touch the tank bottom or its top (if present), side walls of the tank are approximately vertical, and the bottom inclinations are small everywhere, the FDM was derived from the mass and momentum conservation equations based on the Airy wave theory. By neglecting all nonlinear terms occurring in the derivative process of the approach, the Helmholtz equation that combines the complex amplitude of wave elevations in tanks and the complex wave number reads as follows:

$$k_c^2\widehat{h} + \widehat{h}_{xx} + \widehat{h}_{yy} = 0, \tag{1}$$

where subscripts xx and yy represent the second partial derivative in the x- and y-directions, respectively. The hat symbol stands for the complex amplitude; and the complex wave number is defined using wave number k, which is determined via the dispersion relation from Airy wave theory, where l is tank length, d is water depth, and δ is the non-dimensional damping parameter:

$$k_c = k\sqrt{1 - \frac{i\delta kl}{\sinh(kd)}}. \tag{2}$$

We linearized the bottom friction force to include the damping effect of fluid motion in tanks using the non-dimensional parameter δ. Although Qi et al. (2024) determined δ for their model tank, we employed a new method.

Fig. 1 illustrates a control volume applied in the FDM for a rectangular floor plan of area A. The control volume extends from the tank bottom to the fluid's free surface height H. By defining boundary conditions, wall cells were specified as walls (actuators) moving with complex amplitude $\widehat{y}_\omega$ along the y-axis to represent the average shift of wall cells from their central position (piston-type). The relationships between the complex amplitude of the fluid velocity and wall motions moving in the x- and y-directions, respectively, are written as follows:

$$\frac{1}{k}\tanh(kd)\widehat{u} = i\omega\widehat{x}_\omega \text{ and } \frac{1}{k}\tanh(kd)\widehat{v} = i\omega\widehat{y}_\omega. \tag{3}$$

where ω is the circular frequency of a moving control volume.

The grid sensitivity study for the FDM carried out by Qi et al. (2024) employed a cell size of 1.0 cm in the x-direction. As our model tank was similar, we used this same cell sizes. The actuators were located at the two ends of the pool. They started moving from the position shown in Fig. 2 and moved harmonically with an amplitude of up to 70 mm. Thus, the cell size was extended to 70 mm beyond the pool's ends. These extensions also defined the origin of the actuators. Fig. 2 shows the geometric arrangement and the dimensions of the model pool with actuators. The computational domain comprised 39 cells in the x-direction and 139 cells in the y-direction. With these cells, it took less than 0.5 s for the FDM to compute the flow in the pool.

By discretizing the computational domain and applying the boundary conditions, we obtained the geometric distribution of different cell types shown in the top graph of Fig. 3. Grey cells represent the stationary pool boundaries; orange cells, the moving actuators; blue cells, the water in the pool; and white cells, the areas outside the pool. The numbering at the pool's transverse and longitudinal edges identifies dimensional x- and y-coordinates, respectively. They specify the dimensions of the model pool in millimeters, with the associated coordinate system as defined in Fig. 2.

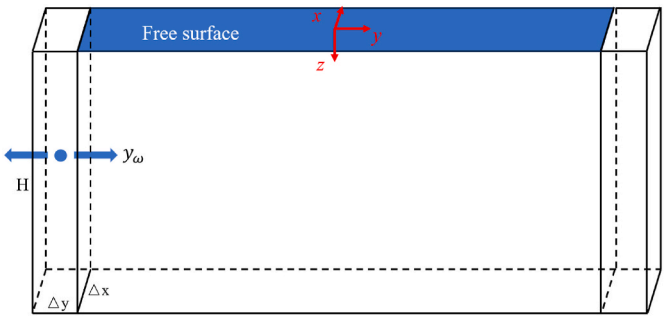

Fig. 1. Illustration of one cell for the piston-type actuator moving along the y-axis.

The two actuators at both pool ends moved harmonically about the original position of sidewalls. The motion amplitudes of the actuators were equal, and they moved with the same phase of $\varepsilon = 0$. Their motion is defined as follows:

$$y_\omega(t) = \mathrm{Re}\{\widehat{y}_\omega e^{(i\omega t+\varepsilon)}\}. \tag{4}$$

The lower graph of Fig. 3 shows representative results (here, the real part of the solutions) caused by a roll excitation of 1.0° and actuator amplitudes of 10 mm oscillating at a period of 4.0 s without a phase difference between the pool's excitation and the actuator motions, and with the water depth set to 0.13 m. The colour bar identifies the computed free surface elevations inside the pool.

2.2. The CFD approach

Using a commercial CFD tool, we performed comparative computations to verify the FDM for cases with moving actuators and to further investigate the feasibility of these actuators to mitigate waves in the pool caused by irregular ship motion-induced excitations. To determine the fluid motions, the CFD code solved the URANS equations for an incompressible fluid and applied the $k-\omega$ SST turbulence model of Menter et al. (2003). To capture the free surface, we utilized the VOF method of Hirt and Nichols (1981) and applied the overset technique to account for the motion of active actuators. The actuators were considered watertight, which meant that no gaps existed between actuators and pool walls. Hence, the no-gap option of the overset-technique had to be activated. Mass conservation may not have been strictly fulfilled for periodic flow, especially when overlapping grids and long aspect-ratio cells were used. Accordingly, we activated the "mass tracking" option to avoid loss of mass in pool.

Fig. 4 shows the geometric arrangement of the model pool colored in grey, and with the actuators colored in blue. The housing of the actuators is 0.2 m high, and the middle of the pool is 0.3 m high to avoid overflow. As shown in the left graph of Fig. 5, the grid is appropriately refined near the free surface. The red rectangle surrounds the overset region. The actuators were originally situated 70 mm outside of the pool's ends, and the amplitude of an actuator motion was limited to 70 mm, which meant that their motion did not extend into the middle of the pool. The right graph of Fig. 5 shows gridding at the face side of the pink overset boundary, whereas the other faces of the overset region are part of the sides of the pool.

A grid sensitivity study was carried out with the pool moving harmonically with a roll amplitude of 1.0° at a frequency of $\pi/2$ rad/s for 60 periods, including a linear time ramp of 10 periods. Actuators on both sides of the pool slide inside the housing moved harmonically with an amplitude of 10 mm at the same frequency of excitation. Wave elevations of a point located at $x = 0.62$ m and $y = 0.0$ m were measured. The amplitude of excited waves was estimated by performing a Fast Fourier Transformation (FFT) using time histories of wave elevations obtained over the last 20 periods.

We adopted a factor of 1.26 for both spatial and temporal refinement to generate three successively finer grids and the associated time steps. Table 1 lists the smallest cell sizes near the free surface, the total number of cells, and the time step for each grid.

Fig. 6 plots wave elevations obtained on the three grids. This asymptotic analysis of the wave amplitudes demonstrated the monotonic convergence for the target solutions. Quantitatively, we calculated the convergence ratio as follows:

$$R = \varepsilon_{32}/\varepsilon_{21}, \tag{5}$$

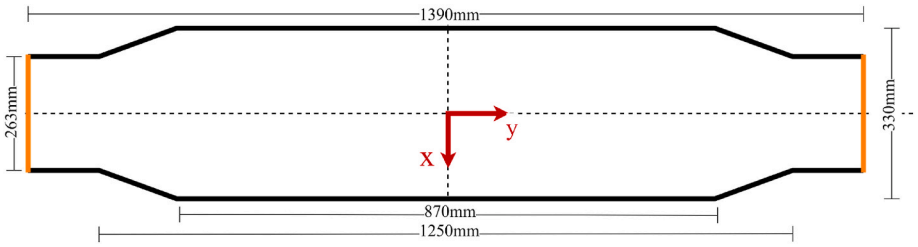

Fig. 2. Geometric arrangement of the model tank with piston-type actuators at its ends.

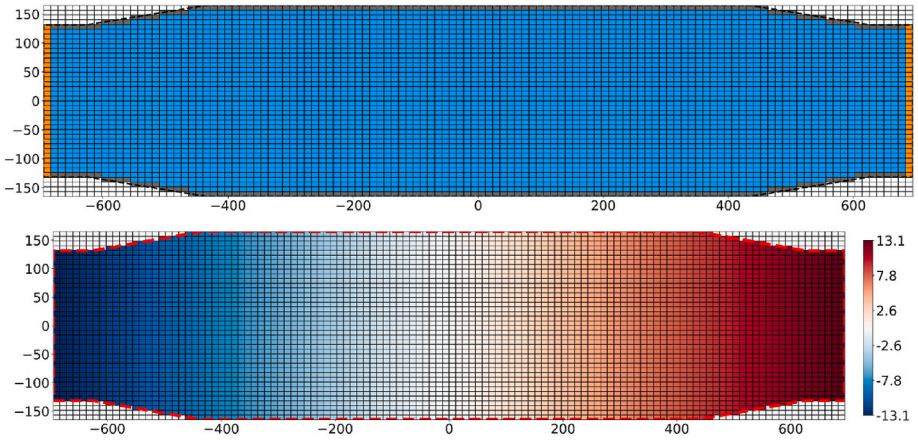

Fig. 3. Cell types according to boundary conditions (top) and computed free surface elevations (bottom) caused by a 1.0° roll excitation and 10 mm actuator amplitudes at a period of 4.0 s with the water depth set to 0.13 m.

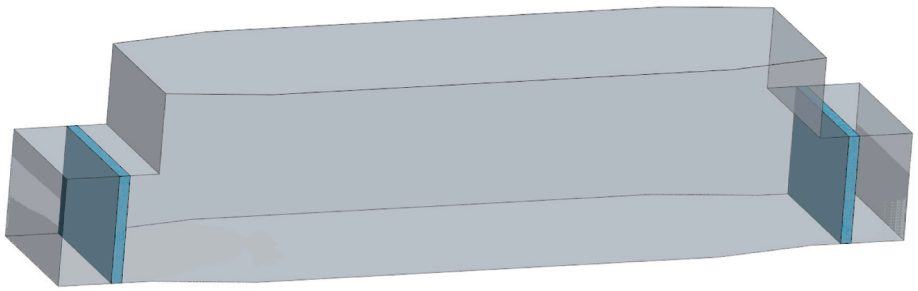

Fig. 4. Geometric arrangement of the model pool with actuators.

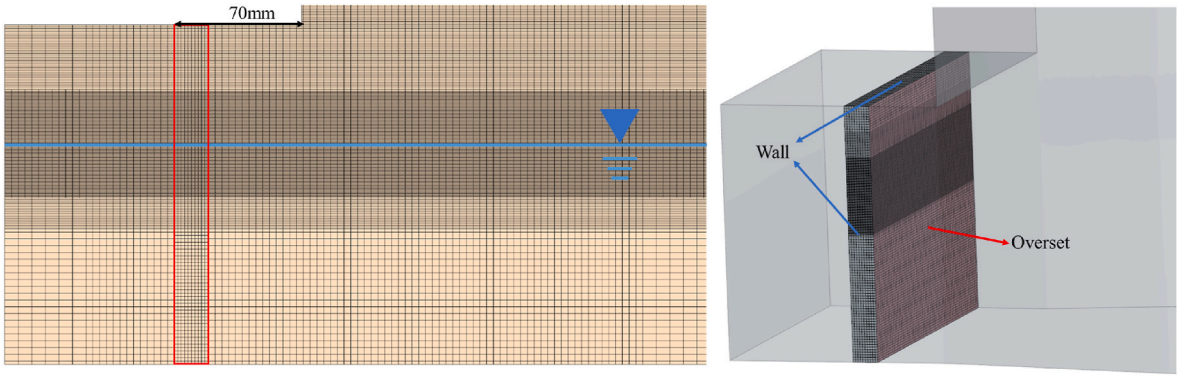

Fig. 5. Grid refinement at the pool's free surface (left) grid details of an actuator (right).

where ε_{32} represents the difference between wave elevations obtained on grids G_3 and G_2 and ε_{21} and the difference between wave elevations obtained on grids G_2 and G_1.

Following the recommendation of the International Towing Tank Conference (ITTC, 2008) and applying the process of Qi et al. (2024) for our grid sensitivity analysis, we estimated the uncertainties and the associated discretization errors in Table 2, where the numerical error δ_{RE}, the order of accuracy p, the correction factor C_F, and the numerical benchmark result S_c, the total discretization uncertainty U_D as well as

Table 1
Cell sizes and number of cells for the three successively finer grids.

Grid	Height Δz [mm]	Length Δx [mm]	Width Δy [mm]	No. of cells [10^6]	Time step [ms]
G_1 (coarse)	1.26	6.60	5.00	0.82	2.52
G_2 (medium)	1.00	5.24	3.97	1.75	2.00
G_3 (fine)	0.79	4.16	3.15	3.45	1.59

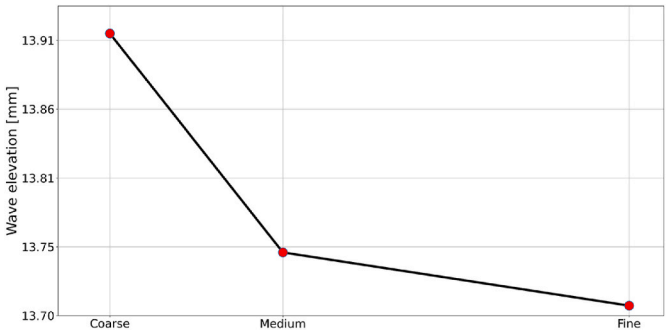

Fig. 6. Wave elevations obtained on the three successively refined grids.

Table 2
Estimated uncertainties and discretization errors.

R	P	C_F	S_C	U_D (%S_C)	Diff_C	Diff_M	Diff_F
0.243	6.118	5.296	13.679	0.930	1.754%	0.513%	0.212%

the difference between wave elevation obtained from different grids were estimated. As seen, carrying out the simulations on the fine grid and using the smallest time step size did not significantly decrease the solutions' uncertainties. Therefore, we performed all subsequent CFD simulations on the medium grid, using the medium time step size of 2.0 ms.

2.3. Determination of δ

Qi et al. (2024) preliminarily determined the parameter δ by comparing wave elevations obtained from the CFD technique and the FDM for periods out of resonance. Therefore, this preliminary damping parameter is valid only at or near resonance. However, here it was necessary to monitor free surface elevations also in violent and braking waves using the CFD approach. Therefore, this value of δ does not cover all frequencies and, consequently, it is not suitable for calculations at resonance. Thus, we determined the damping factor that also consider cases at resonance.

Using the FDM approach, we obtained wave elevations over a broad range of frequencies for a roll excitation of 0.5° and a sway excitation of 0.025 m. Fig. 7 plots the resulting wave elevations, where the damping factor was specified as 0.01. Based on these wave elevations, the natural frequency of the model pool was estimated to be 2.62 rad/s, which corresponded to an eigenperiod of 2.4 s.

As described by Qi et al. (2024), bottom friction force F_R acting along in the y-axis, assumed to be linearly proportional to the fluid velocity u in the y-direction, was expressed as follows:

$$F_B = Al\omega\rho\delta u, \tag{6}$$

where A represents the area of a cell and ρ the density of the fluid. Equation (6) is valid solely under the condition that the fluid within the model pool maintains a laminar regime. By employing a characteristic length L of 1.25 m and a maximal flow velocity along the y-direction of 0.2 m/s obtained from a test case of CFD computation (see Fig. 9), the Reynolds number (Re) is calculated as approximately 2.8×10^5 using the formula

$$\text{Re} = \frac{\rho u L}{\nu}, \tag{7}$$

where ν represents dynamic viscosity of water. In comparison to the critical Reynolds number for flow on plates (5×10^5), the laminar regime condition is satisfied.

We used the numerical model pool shown in Fig. 4 and refined the grid near the pool bottom to keep the y plus smaller than unity, i.e., a wall function was not applied. We carried out CFD simulations for a roll excitation of 0.5° at periods between 2.4 and 3.0 s in steps of 0.1 s. In this series of simulations, both actuators remained stationary. The fluid velocity in the y-direction varied between pool bottom and free surface. Fig. 8 depicts the distribution of these fluid velocities, and the attached colour bar quantifies them. As the velocity of air (colored deep blue in the upper region of the velocity distribution) was not monitored, we averaged the monitored velocity from the bottom up to the fluid free surface at the centre of the pool.

Representatively, Fig. 9 plots the bottom friction force as a black dotted line and the averaged water velocity in the y-direction as a blue solid line for the simulation obtained at a period 2.4 s. We obtained the amplitudes of the bottom friction force by applying the FFT analysis for

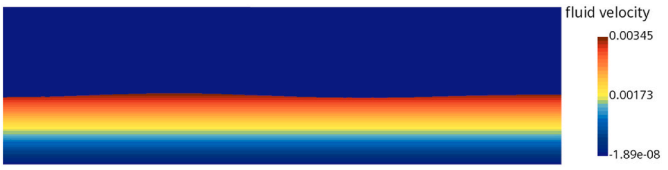

Fig. 8. Water velocities in the y-direction relative to the pool bottom.

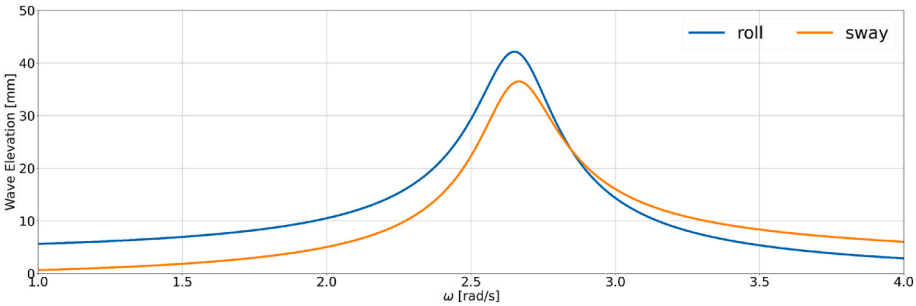

Fig. 7. Wave elevations at broad frequencies for roll and sway obtained from the FDM approach.

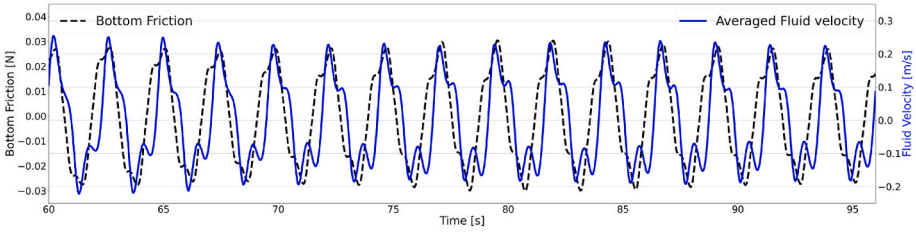

Fig. 9. Bottom friction force and averaged fluid velocity in the *y*-direction at a period of 2.4 s.

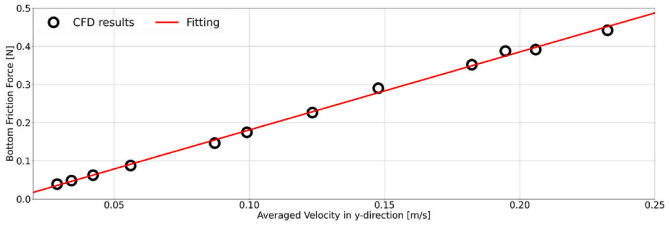

Fig. 10. Relationship between the bottom friction force and the averaged velocity in *y*-direction.

time histories between 32 and 52 periods.

Fig. 10 presents the relationship between the monitored bottom friction force and the averaged water velocity in *y*-direction. The red line represents the corresponding linear fitting line. The slope a of this line turned out to be 2.044, and the associated R squared value was 0.998. Knowing that $a = Al\omega\rho\delta$, we evaluated the value of δ to be 0.004 by substituting values for the area A of the bottom and the natural frequency ω of the pool. We used this value for all subsequent FDM calculations.

3. Experimental model tests

In the sloshing laboratory, experimental tests were carried out for a model pool equipped with active actuators to validate the FDM. Fig. 11 shows a photo of the model pool situated on the platform. This platform was able to move in six degrees-of-freedom. Two metal housings covered the actuators at both sides of the pool. On each side of the pool, the two actuators were separated by a thin metal plate placed inside the metal housing. Rubber seal rings ensured that the area behind the actuators remained watertight. In all experimental test cases, the motions of the two actuators were the same.

Fig. 12 shows wave probes installed along the walls of the pool. These probes extended from the pool's bottom to a height of 0.195 m. These wave probes adequately covered the test measurements. Measured were small excitation amplitudes and actuator motions at frequencies outside the range of the pool's resonance frequencies. These 24 wave probes were arranged symmetrically about the pool's longitudinal centre line. Only the 20 probes marked in orange in Fig. 12 were activated to measure free surface elevations, whereas probes WP13, WP14, WP27, and WP28 were fixed on the surface of the actuators to move with the actuators.

4. Test case description

4.1. Numerical tests

We performed CFD simulations under various amplitudes of excitation motions and of actuator motions at different frequencies outside the lowest natural frequency of the model pool, which frequency was estimated to be 3.0 rad/s. A roll amplitude of 1.0° and a sway amplitude of 0.025 m were tested. In addition, simultaneous roll and sway excitations were considered for actuator amplitudes of 10 and 20 mm, with the phase difference between roll and sway excitations of $\varepsilon = 0$. Each simulation ran for 60 periods in total, including a linear ramp simulation of 10 periods. Based on these conditions, the CFD approach specified the excited roll motion, for example, as follows:

$$\varphi(t) = \begin{cases} |\widehat{\varphi}|\sin\left(\frac{2\pi}{T}t + \varepsilon_{\varphi}\right)\ \frac{t}{10T}, t \le 10T \\ |\widehat{\varphi}|\sin\left(\frac{2\pi}{T}t + \varepsilon_{\varphi}\right), t > 10T \end{cases}, \tag{8}$$

with the phase angle for roll of $\varepsilon_{\varphi} = 0$. This corresponded to the following input of roll excitation in the FDM approach:

$$\widehat{\varphi} = (|\widehat{\varphi}| + 0j). \tag{9}$$

A period of 3.0 s, regarded as close to the eigenperiod of the pool, was also considered for a simultaneously excited roll motion to observe the performance of the FDM approach under resonance conditions. Wave elevations were monitored in the CFD simulations at positions of the wave probes in the model tests (see Fig. 12). Note that the phase of all excitation and actuator motions was specified as $\varepsilon = 0$. For simultaneous roll and sway excitations, the actuator amplitudes of 10 and 20 mm were investigated. Table 3 summarizes the test conditions considered.

4.2. Experimental tests

We performed model tests only for the roll excitation of 1.0° at

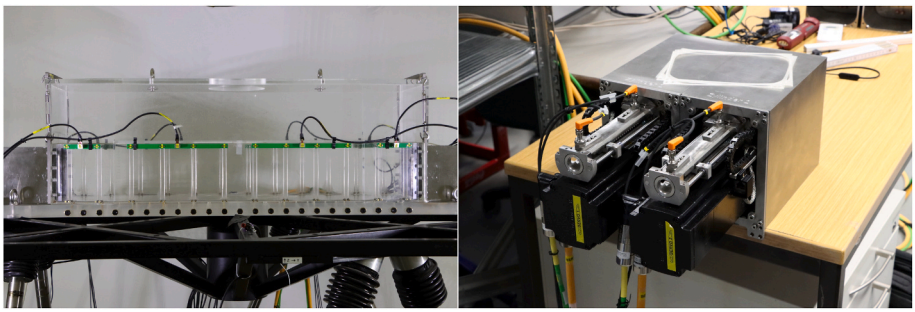

Fig. 11. Photo of the model pool (left) and the actuators (right).

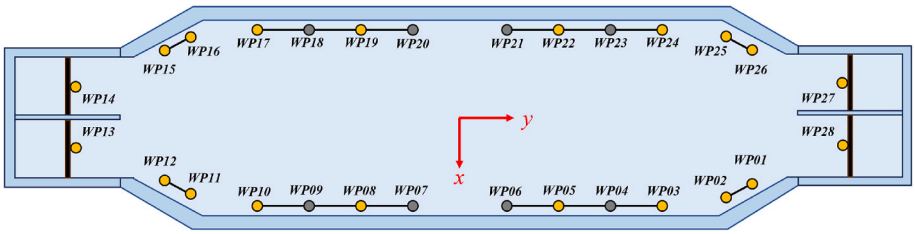

Fig. 12. Arrangement of wave probes situated in the model pool.

frequencies outside the range of the pool's resonance frequencies. For each case, tests were conducted for a total of 125 excitation periods, which included a linear time ramp of eight periods. Amplitudes of actuator motions varied from 0 to 20 mm, and the phase difference between pool and actuator motions was $\varepsilon = 0$ for all cases. Table 4 summarizes the test conditions considered.

Differing from the model applied in the CFD approach, the origin of the coordinate system in the experiments was set at the centre of the platform. As the thickness of the pool bottom) was 40 mm below the inner surface of the pool bottom, the coordinate system in the FDM had to be shifted 40 mm downwards to be compatible with the test conditions.

5. Validation of the FDM

To validate the FDM, we determined comparable time histories of the excited free surface wave elevations by transforming the frequency domain results obtained from the FDM into comparable time domain simulations via FFT analyses using the following expression:

$$h(t) = \mathrm{Re}\{\widehat{h}e^{i\omega t}\}. \tag{10}$$

This also verified the FDM results, which were obtained in the frequency domain. This enabled comparing the FDM results, transformed into the time domain, with results obtained from the CFD approach as well as with experimental measurements. We mostly focused on wave elevations at wave probes WP01 and WP13. Due to the limitation of the linear FDM, deviations between results from the FDM and comparable measurements of less than 10% were acceptable for validation purposes.

5.1. Comparison between FDM and CFD results

For the roll excitation of 1.0° and an actuator amplitude of $\alpha = 10$ mm, Fig. 13 plots comparative time histories obtained at periods of 4.0 and 6.0 s under non-resonance conditions obtained from 20 to 40 periods. The top graph of Fig. 13 shows that, for simulations at the 4.0 s period, both approaches determined free surface elevations that compared favorably with each other. Only of slight differences are visiable at wave probe WP13 (Fig. 13 top right). At the 6.0 s period, the predicted free surface elevations from both approaches could hardly be distinguished at both monitored wave probes WP01 and WP13 (Fig. 13 bottom). Fig. 14 plots time histories for the other cases, obtained with amplitudes of actuator motions of 30 and 40 mm. Here, too, the wave elevations predicted by the two approaches hardly differed from each other. Only slight differences occurred. The left graph of Fig. 14 plots time series that were obtained at a longer period of 8.0 s. Note that, for such a case, the free surface elevation of the excited waves in the pool were less harmonic than those at the shorter periods of 4.0 and 6.0 s plotted in Fig. 13. Nevertheless, the amplitudes and frequencies of free surface elevations obtained from the FDM and from the CFD technique still compared favorably to each other.

Table 3
Numerical test conditions.

Excitation	roll 1°	sway 0.025m	roll 1° and sway 0.05m	Number of cases
Period [s]	3.0–8.0	4.0–8.0	3.0–8.0	56
Actuators [mm]	10.0, 20.0, 30.0, 40.0		10.0, 20.0	

Table 4
Model test conditions.

Excitation	roll 1°	Number of cases
Period [s]	4.0, 5.0, 6.0, 7.0, 8.0	15
Actuators [mm]	0.0, 10.0, 20.0	

Contrary to the cases with periods well outside of the pool's resonance region, for a case with a period of 3.0 s, i.e., a case closer to resonance, the performance of the FDM was barely satisfactory. Fig. 15 plots time histories of free surface elevations obtained from the FDM and the CFD technique for a 1.0° roll amplitude and an actuator amplitude of $\alpha = 10$ mm. Although their frequencies compared favorably, the amplitudes from the CFD simulations exceeded those from the FDM, especially the elevation at WP13, which was attached to an actuator. This indicated that nonlinearities affected the free surface elevations. (Recall that the CFD technique accounts for nonlinear effects.)

Fig. 16 plots comparable time histories for the two cases with larger actuator amplitudes of $\alpha = 30$ and 40 mm, again obtained from the FDM and the CFD simulations for a 1.0° roll amplitude. As seen, for these latter cases the excited free surface elevations monitored at WP01 were significantly damped compared with those obtained for the smaller actuator amplitude of $\alpha = 10$ mm. Nevertheless, differences between predictions from the FDM and the CFD simulations remained although, as seen in the right graph of Fig. 16, these differences decreased with decreasing free surface elevations.

Table 5 provides a summary of the percentage deviation of wave elevations derived from the FDM and the CFD approach for roll excitation across different amplitudes of actuators. Notably, outside of the resonance, the FDM demonstrates favorable predictions, exhibiting deviations against the CFD approach of less than 5%. However, near the resonance, indicated in red within Table 5, deviations exceeding 20% were observed.

For sway excitations, the FDM approach yielded almost the same free surface elevations from the excited waves for most cases as the CFD approach. Representatively, Fig. 17 plots comparable time histories of wave-excited free surface elevations monitored at WP01 for the two test conditions specified by a 0.025 m sway amplitude and actuator amplitudes of $\alpha = 10$ mm at a period of 4.0 s (left) and $\alpha = 30$ mm at a period of 6.0 s. Although not plotted here, time histories at the other wave probes demonstrated the favorable agreement between the two approaches.

For simultaneous roll and sway excitations, Fig. 18 plots comparative time histories of wave elevations obtained from the FDM and CFD simulations and actuator amplitudes of $\alpha = 10$ mm at a period of 3.0 s and $\alpha = 20$ mm at a period of 6.0 s. The 10 % deviations between the two approaches of roll-induced wave elevations obtained from the FDM for the 1.0° roll amplitude case at a period of 3.0 s, plotted in the left graph of Fig. 15, i.e., for simultaneous excitation at a period close to the pool's resonance frequency, turned out to be similar. For excitations at

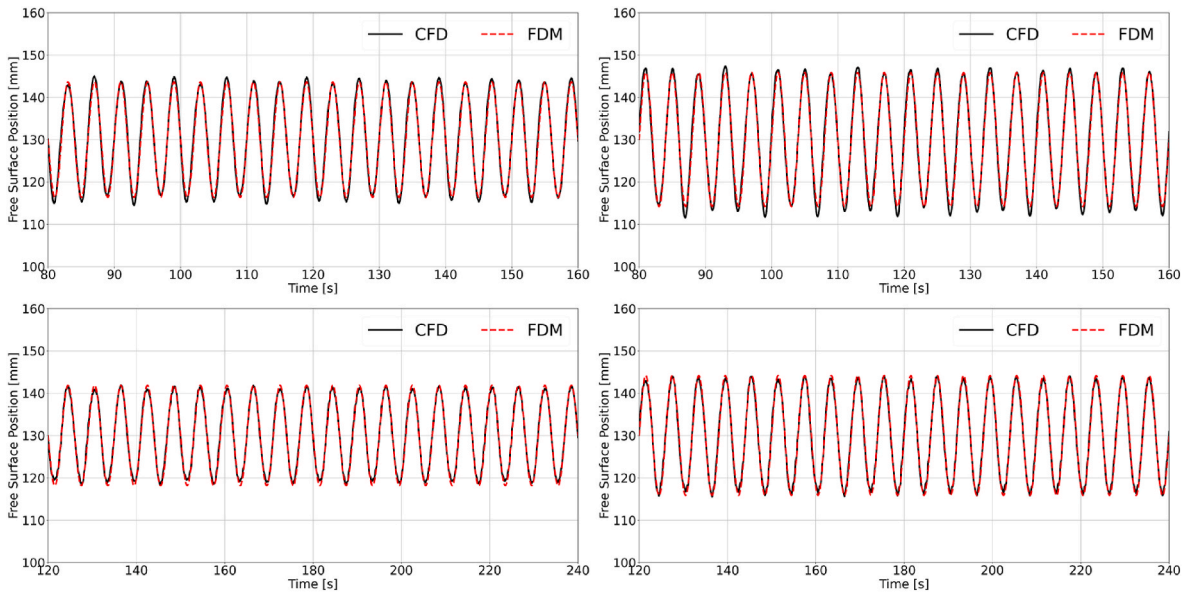

Fig. 13. Comparative time histories of free surface elevation at WP01 (left) and WP13 (right) obtained from the FDM and the CFD simulations for a 1.0° roll amplitude and an actuator amplitude of α = 10 mm at a period of 4.0 s (top) and 6.0s (bottom).

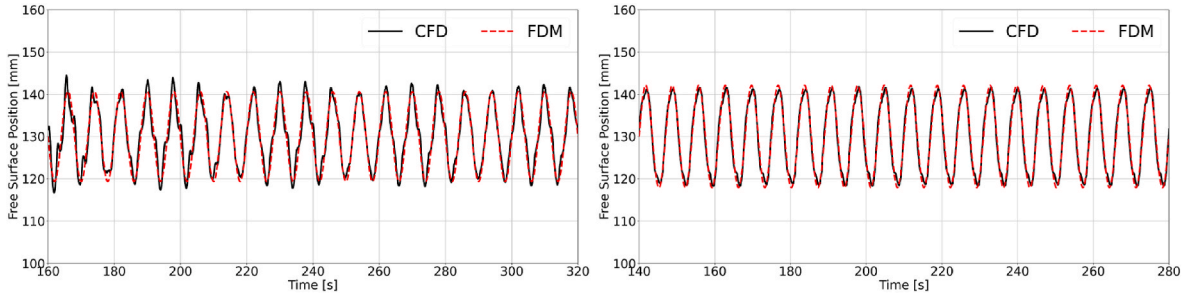

Fig. 14. Comparative time histories of free surface elevation at WP01 (left) and WP13 (right) obtained from the FDM and CFD simulations for a 1.0° roll amplitude and an actuator amplitude of $\alpha = 30$ mm at period of 8.0 s (left) and for an actuator amplitude of $\alpha = 40$ mm at a period of 7.0 s (right).

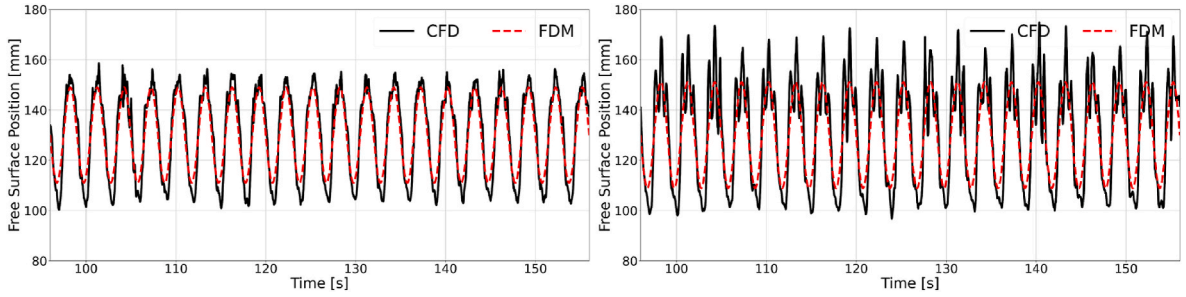

Fig. 15. Comparable time histories of free surface elevation at WP01 (left) and WP13 (right) obtained from the FDM and the CFD simulations for a 1.0° roll amplitude and an actuator amplitude of $\alpha = 10$ mm at a period of 3.0 s.

frequencies away from the pool's resonance frequency, the FDM approach yielded nearly identical predictions.

Fig. 19 plots comparative roll- and sway-induced free surface (wave) elevations at WP01 versus the pool's excitation period for actuator amplitudes of $\alpha = 10$, 20, 30, and 40 mm. Crosses mark results from the FDM; circles, results from the CFD simulations. As seen, results obtained from the two approaches were similar, especially at periods away from resonance, where the FDM results deviated by less than 3 % from the CFD predictions. Relatively large underpredictions exceeding 10 % resulted from the FDM for cases at a period of 3.0 s. Detailed data presented in Fig. 19 can be found in Table 6, where the wave elevations are listed in millimeters (mm). At all other wave probes, free surface (wave) elevations were similar.

These comparative results from the CFD approach demonstrate that the FDM yielded precise predictions of waves in the pool with actuators oscillating at periods outside the pool's resonance frequency. Of course, for periods near the pool's resonance frequency range, the FDM was not expected to yield accurate predictions.

5.2. Comparison between FDM results and model test measurements

For the roll excitation of 1.0° and an actuator amplitude of $\alpha = 10$

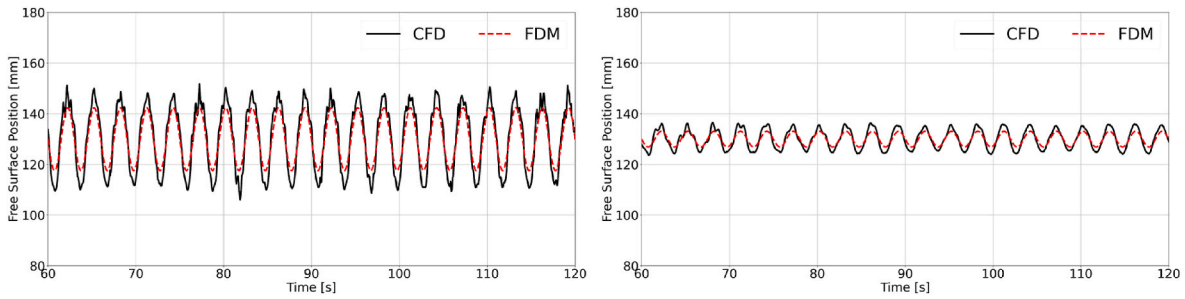

Fig. 16. Comparative time histories of free surface elevation at WP01 obtained from the FDM and the CFD simulations for a 1.0° roll amplitude and actuator amplitudes of $\alpha = 30$ mm (left) and $\alpha = 40$ mm (right).

Table 5
Deviations of wave elevations obtained from the FDM and the CFD simulations for roll excitation at WP01.

Excitation	Actuator Amplitude [mm]	Deviation [%]					
		T = 3s	T = 4s	T = 5s	T = 6s	T = 7s	T = 8s
Roll	10	−20.68	−6.15	−5.52	−3.74	−2.72	−2.02
	20	−22.77	−5.77	−4.99	−3.28	−2.32	−1.74
	30	−25.87	−6.91	−4.89	−3.11	−2.17	−1.61
	40	−24.89	−5.35	−3.99	−3.04	−2.07	−1.51

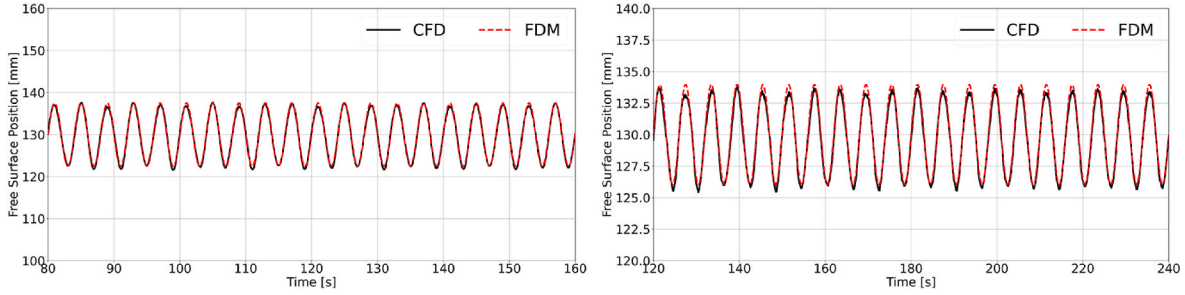

Fig. 17. Comparative time histories of free surface elevation at WP01 obtained from the FDM and the CFD simulations for a 0.025 m sway amplitude and actuator amplitudes of $\alpha = 10$ mm at a period of 4.0 s (left) and $\alpha = 30$ mm at a period of 6.0 s (right).

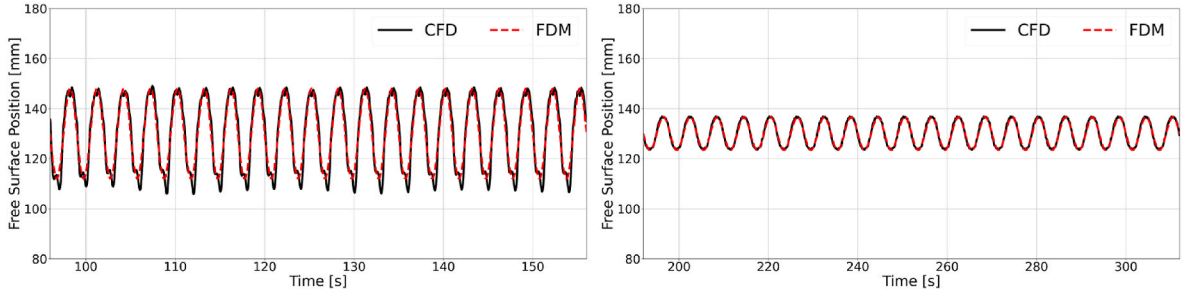

Fig. 18. Comparative time histories of free surface position at WP01 obtained from the FDM and CFD simulations for a simultaneous roll and sway excitation and actuator amplitudes of $\alpha = 10$ mm at a period of 3.0 s and $\alpha = 20$ mm at a period of 6.0 s.

mm, comparative time histories of free surface elevation at WP01 were obtained from the FDM and from model test measurements (EXP) for a 1.0° roll amplitude. Fig. 20 plots the two time series determined when the pool oscillated at periods of 4.0 and 5.0 s; Fig. 21, when the pool oscillated at periods of 6.0 and 7.0 s, with the actuator amplitude increased to 20 mm. As seen, the resulting free surface amplitudes at these four periods compared favorably to each other. These results demonstrate the favorable performance of the FDM as this method was able to predict harmonic time histories of roll-excited waves in the pool with an accuracy of less than 5 %, provided the pool was excited at a frequency out of its resonance frequency range.

Fig. 22 plots comparative roll-induced free surface (wave) elevations at WP01 versus the pool's excitation period for actuator amplitudes of $\alpha = 10$ and 20 mm. Crosses mark results from the FDM; circles, results from the experiments. Black dotted lines connect results from the FDM; blue dotted lines, results from the experiments. As seen, at an actuator amplitude of $\alpha = 10$ mm, the largest deviation (around 10 %) from measurements of an FDM predicted elevation occurred at the 6.0 s period, whereas at an actuator amplitude of $\alpha = 20$ mm, the largest deviation (around 12%) from measurements of an FDM predicted elevation occurred at the 4.0 s period. At the other periods, the FDM predictions deviations from measurements were considerably smaller.

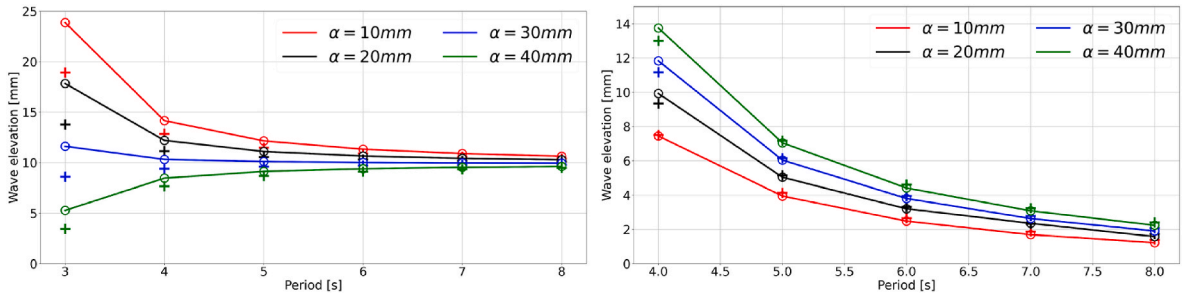

Fig. 19. Comparative free surface (wave) elevations at WP01 obtained from the FDM and the CFD simulations for roll (left) and sway (right) and actuator amplitudes of $\alpha = 10$ mm, $\alpha = 20$ mm, $\alpha = 30$ mm, and $\alpha = 40$ mm vs. excitation periods.

Table 6
Wave elevations obtained from the two approaches for roll and sway excitation at WP01.

Excitation	Actuator Amplitude [mm]	T = 3s		T = 4s		T = 5s		T = 6s		T = 7s		T = 8s	
		FDM	CFD	FDM	CFD	FDM	CFD	FDM	CFD	FDM	CFD	FDM	CFD
Roll	10	18.94	23.88	12.86	14.16	11.48	12.15	10.90	11.33	10.60	10.90	10.42	10.63
	20	13.77	17.84	11.13	12.20	10.54	11.10	10.30	10.65	10.18	10.42	10.10	10.28
	30	8.61	11.61	9.40	10.31	9.61	10.10	9.70	10.02	9.76	9.97	9.79	9.95
	40	3.45	5.28	7.67	8.46	8.67	9.13	9.10	9.39	9.34	9.53	9.48	9.62
Sway	10	–	–	7.50	7.64	4.13	3.98	2.66	2.53	1.87	1.82	1.39	1.44
	20	–	–	9.34	9.94	5.14	5.22	3.31	3.21	2.33	2.16	1.74	1.86
	30	–	–	11.17	11.79	6.15	6.32	3.96	4.09	2.79	2.60	2.08	1.99
	40	–	–	13.00	13.92	7.16	7.01	4.61	4.44	3.24	3.12	2.42	2.50

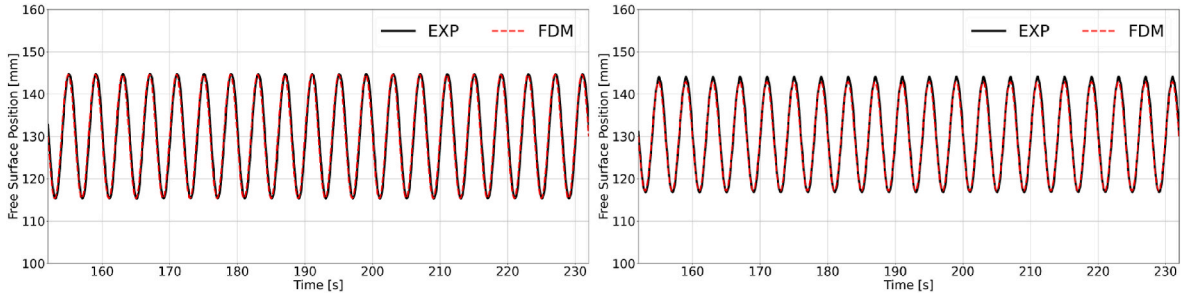

Fig. 20. Comparative time histories of free surface elevation at WP01 obtained from the FDM and model test measurements (EXP) for a 1.0° roll amplitude at a period of 4.0 s (left) and 5.0 s (right) and an actuator amplitude of $\alpha = 10$ mm.

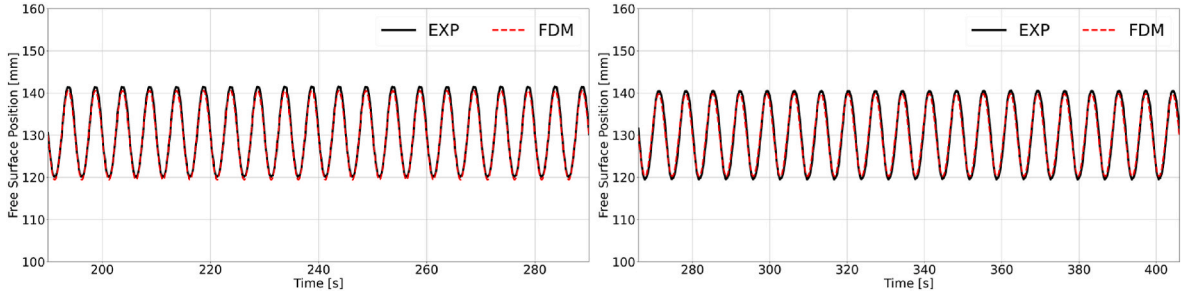

Fig. 21. Comparative time histories of free surface elevation at WP01 obtained from the FDM and model test measurements (EXP) for a 1.0° roll amplitude at a period of 6.0 s (left) and 7.0 s (right), and an actuator amplitude of $\alpha = 20$ mm.

Although deviations between the FDM predictions and measurements varied from sensor to sensor, they were mostly less than 10 %. Detailed data presented in Fig. 22 can be found in Table 7, where the wave elevations are listed in millimeters (mm). Based on these comparisons with measurements, we considered the FDM approach to be validated for periods outside the pool's resonance range.

6. Optimum actuator amplitudes

Applying the FDM approach, we further investigated the feasibility of mitigating excited waves in the pool using active actuators situated on the pool's ends. For such cases, Fig. 23 plots time histories of measured wave elevations caused by a 1.0° roll amplitude at a 4.0 s period and actuator amplitudes of $\alpha = 0$, 10, and 20 mm. As seen, the actuators did

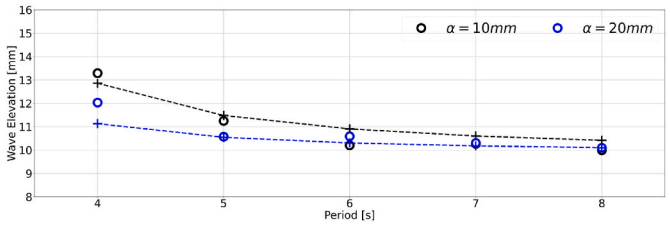

Fig. 22. Comparative free surface (wave) elevations at WP01 obtained from the FDM (+) and from model test measurements (○) for a 1.0° roll amplitude and actuator amplitudes of $\alpha = 10$ mm and $\alpha = 20$ mm vs. excitation period.

dampen the wave elevations in the pool. However, this small damping did not significantly mitigate the waves in the pool. Hence, the actuator amplitudes had to be increased to more effectively dampen the excited waves.

Fig. 24 presents two plots of wave elevation versus actuator amplitude obtained from the FDM caused by a 1.0° roll amplitude of the ship. The differing line colours represent the periods of actuator oscillations: The left-hand plot refers to the actuators oscillating at periods outside of resonance, i.e., at T = 4.0, 5.0, 6.0, 7.0, and 8.0 s, whereas the right-hand plot refers to actuator oscillating at periods only near resonance, i.e., at T = 2.6, 2.8, and 3.0 s. Recall that the phase difference between roll excitation and actuator motions remained zero. As seen, at certain actuator periods, the excited wave elevation decreased with increasing actuator amplitude, and then the wave elevation was linearly proportional to actuator amplitude. For example, for the actuators oscillating at the period of T = 4.0 s with an amplitude of 80 mm, free surface (wave) elevations were mitigated to almost zero. In contrast, for the actuators oscillating at the period of T = 8.0 s, the pool's free surface was hardly damped at all although the actuator amplitudes of 80 mm did not change.

As shown, the FDM did not perform well for cases near resonance. Of course, this was due to its theoretical limitations, and its predictions of mitigated wave elevation in the pool deviated by over 10 %. Nevertheless, we used this method to obtain a general overview to what extent active actuators are able to mitigate excited waves in a swimming pool onboard ship. The right-hand plot of Fig. 24 relates free surface (wave) elevation and actuator amplitude at periods near resonance, albeit for roll excitation of 0.5°. As seen, for each period considered, actuator amplitudes were found for which the excited waves in the pool are most effectively damped. Furthermore, these optimum actuator amplitudes for mitigating waves in the pool decreased at smaller actuator periods.

Fig. 25 presents result from a successful example of mitigating the excited waves in the pool. The left-hand plot refers to FDM results for simultaneous excitations of 1.0° roll amplitude and 0.05 m sway amplitude with the actuators oscillating at periods outside of resonance, specifically, at periods of T = 3.0, 3.5, 4.0, and 5.0 s. As seen, the FDM predictions yielded optimum actuator amplitudes of 22 mm at the actuator period of T = 4.0 s. We performed a comparative CFD simulation with this same amplitude and period of the actuators and plotted the resulting free surface positions at WP01 as time histories. As seen, the agreement between the FDM predicted and the CFD simulated free surface positions at WP01 was favorable, demonstrating that the excited waves were effectively mitigated from an elevation of 4.7 mm down to 0.58 mm. However, as shown in the left-hand plot of Fig. 25, at certain actuator periods, notably at T = 3.0 s, no suitable actuator amplitudes were found at which the excited waves in the pool were efficiently damped. In such conditions, it may be necessary to consider the phase difference between the actuators and the excitation motions to obtain the optimum actuator amplitudes.

Due to the limitation of the FDM, it was challenging to precisely predict excited waves at periods close to the pool's resonance frequency. When nonlinearities became dominant, the FDM predictions were unreliable and the FDM lost its advantage. Nevertheless, we examined whether our FDM was effective in determining the influence of the actuators to mitigate the excited waves in the pool. Therefore, we employed the FDM also for cases at or near the pool's resonance frequency and, concurrently, to investigate the feasibility of using piston-type actuators also under critical conditions.

As seen in the right-hand plot of Fig. 24, at the actuator period of T = 3.0 s, the FDM predicted wave elevation of 23.0 mm at WP01 was mitigated down to 0.16 mm. Fig. 26 presents comparative time histories of FDM predicted and CFD simulated time histories of free surface (wave) positions at WP01 for the case of the actuators oscillating at a period of T = 3.0 s. These time histories illustrate the difference between the cases with and without actuators, i.e., they reinforce the effectiveness of the actuators in that the free surface position at WP01 was damped only when the actuators were operating, here for an amplitude of $\alpha = 23$ mm. Although not large, some deviations between results with actuators obtained from the FDM and the CFD simulations occurred. Summarizing, at periods near the pool's resonance periods, these piston-type actuators did efficiently mitigate the excited waves in the pool, with the FDM here obtaining the optimum actuator amplitudes.

Fig. 1 presents FDM predicted and CFD simulated time histories of free surface (wave) position at WP01 for a 0.5° roll amplitude and with actuator amplitudes of $\alpha = 10$, 16, and 20 mm oscillating at a period of 2.5 s. As seen, the actuators oscillating with an amplitude of $\alpha = 16$ mm mitigated the FDM predicted surface positions down to 0.22 mm. However, the comparative CFD simulations, identified by the blue dotted curve, deviated from the FDM predictions, identified by the red curve. We suspect this deviation occurred because the specified 16 mm amplitude of the actuators was not the most effective, i.e., the optimum amplitude for this case. Therefore, we performed additional CFD simulations with the 10 and 20 mm actuator amplitudes, identified by the solid and dotted green curves, respectively, in Fig. 27. Obviously, actuator operations with amplitudes larger than 16 mm would have reduced free surface elevations further. Although the FDM approach was unable to yield reliable predictions at the pool's resonance period, it did efficiently obtain the optimum actuator amplitudes to mitigate the excited free surface (wave) elevations.

7. Conclusion

We applied our FDM to predict free surface waves excited in a shipboard pool equipped with two piston-type actuators situated at the pool ends. To determine the damping parameter δ of the FDM required evaluating the dependence of mean fluid velocities on bottom friction. We verified and validated our FDM against comparative CFD simulations and experimental model test measurements under various conditions and actuator amplitudes. Our FDM yielded predictions that deviated by less than 10 % from comparable CFD simulations, albeit only at periods outside the eigenperiod of waves excited in the pool. In the resonance of the pool, the CFD approach offers superior predictions

Table 7
Wave elevations obtained from the two approaches for roll and sway excitation at WP01.

Excitation	Actuator Amplitude [mm]	T = 4s		T = 5s		T = 6s		T = 7s		T = 8s	
		FDM	EXP	FDM	EXP	FDM	EXP	FDM	EXP	FDM	EXP
Roll	10	12.86	13.38	11.48	11.29	10.90	10.17	10.60	10.25	10.42	10.05
	20	11.13	12.30	10.54	10.63	10.30	10.84	10.18	10.37	10.10	10.24

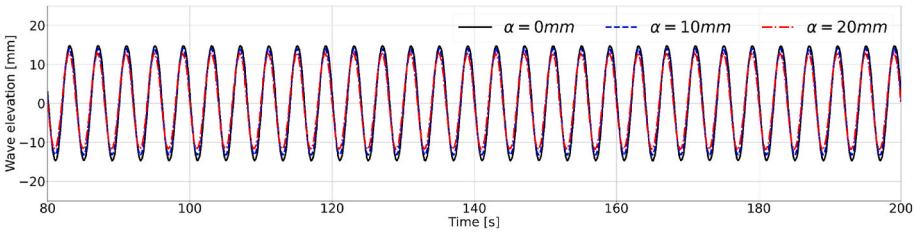

Fig. 23. Comparative free surface (wave) elevations at WP01 obtained from measurements for a 1.0° roll amplitude at a period 4.0s and actuator amplitudes of $\alpha = 0$, $\alpha = 10$, and $\alpha = 20$ mm.

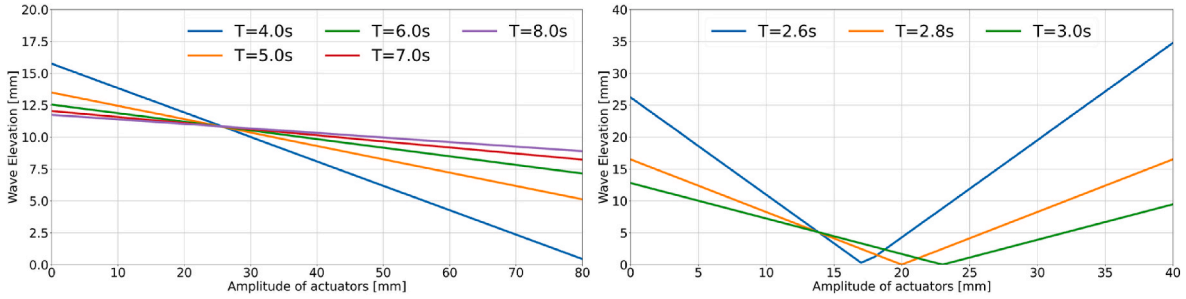

Fig. 24. Free surface (wave) elevation vs. actuator amplitude for the actuators oscillating at periods outside of resonance (left) and near resonance (right).

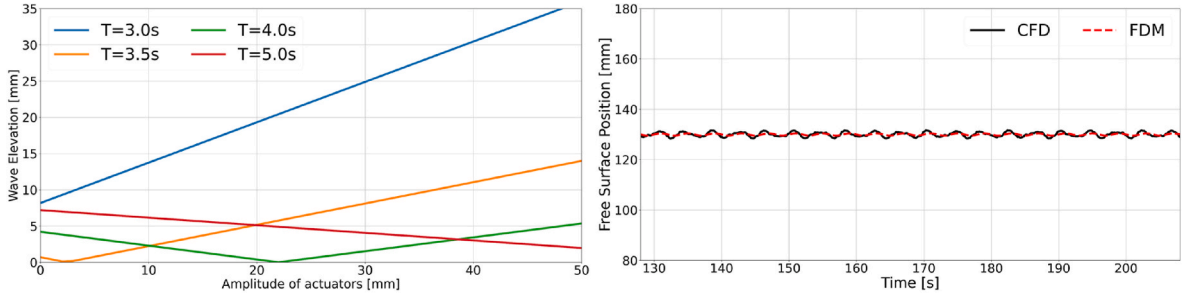

Fig. 25. FDM predicted free surface (wave) elevation vs. actuator amplitude (left) and comparative time histories of mitigated free surface positions at WP01obtained from the FDM and CFD simulations (right) for a 1.0° roll and a 0.05 m sway amplitude with the actuators oscillating at a period of T = 4.0 s.

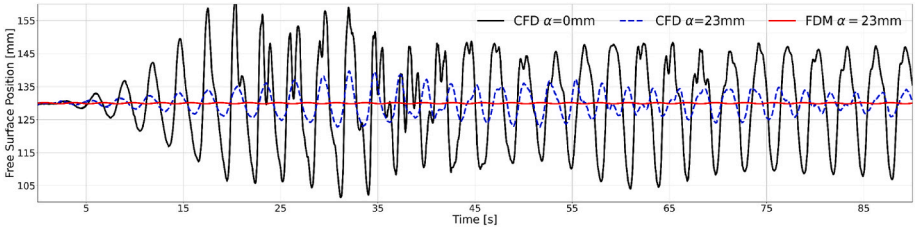

Fig. 26. FDM predicted and CFD simulated time histories of free surface (wave) positions at WP01 for actuator amplitudes of $\alpha = 0$ and $\alpha = 23$ mm and with the actuators oscillating at a period of 3.0 s.

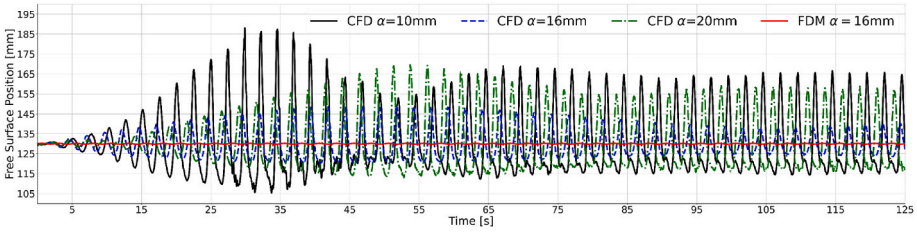

Fig. 27. FDM predicted and CFD simulated time histories of free surface (wave) position at WP01 for a 0.5° roll with actuator amplitudes of $\alpha = 10$ mm, $\alpha = 16$ mm, and $\alpha = 20$ mm oscillating at a period of 2.5 s.

of excited waves, particularly when considering nonlinear effects that our method currently cannot address. Nevertheless, the primary advantage of our FDM lies in its computational efficiency compared to employing a CFD approach utilizing the VOF method and the overset technique. Furthermore, when compared to model tests, our FDM approach demonstrates an accuracy of prediction within less than 10%.

Due to the extremely low computational effort required by the FDM, we are able to generate a preview of excited waves in pools with the effect of piston-type actuators situated at the pool ends under various conditions. This capability aligns with our original intention in developing this approach. For periods outside the pool's resonance range, our approach accurately predicted the mitigated waves and was able to determine the optimum amplitude of the actuators needed to mitigate such waves. For instance, by employing piston-type actuators with an amplitude of 22 mm, waves generated by a simultaneous roll of 1° and sway of 0.05m at a period of 4s can be effectively suppressed to nearly zero, agreeing with results obtained from the CFD approach. However, under certain conditions, we found that the piston-type actuators we considered were unable to mitigate waves excited in the pool, indicating that no optimum actuator amplitudes existed for those scenarios. In such cases, the phase between excitations and the actuators may need to be considered in further investigations. Additionally, under long-period ship motion-induced roll excitations, impractically large actuator amplitudes would be required to mitigate the waves excited in the pool.

We also attempted to estimate the optimum amplitude of actuators for the tank near resonance using the FDM, fully aware of its limitations in addressing nonlinear effects. Despite significant deviations in predicted wave elevations compared to the CFD results, the optimum actuator amplitude predicted by the FDM closely matched that from the CFD approach. In the investigated scenario, we observed a notable reduction in wave elevations from over 100 mm to less than 10 mm with an actuator amplitude of only 16 mm, underscoring the feasibility of piston-type actuators in effectively mitigating excited waves during resonance.

Inspired by this successful attempt to predict the optimum actuator amplitude near resonance, it may be possible to apply the FDM for systematic investigations on the effects of piston-type actuators on wave mitigation in pools excited by ship motions. This could involve diverse pool geometries, water depths, phase differences between actuators and excitation motion, as well as other pertinent parameters. It is important to note that, at the current stage, our FDM provides accurate predictions only outside of resonance. Moving forward, further development of the approach to address nonlinear effects and other potential applications of the FDM will be necessary.

CRediT authorship contribution statement

Yan Qi: Writing – original draft, Visualization, Validation, Software, Resources, Methodology, Investigation, Formal analysis, Data curation, Conceptualization. **Heinrich Söding:** Writing – review & editing, Supervision, Software, Resources, Methodology, Formal analysis. **Jasmin Stöcker:** Resources, Data curation. **Marcel Zydeck:** Resources, Data curation. **Jens Neugebauer:** Resources, Data curation. **Ould el Moctar:** Writing – review & editing, Supervision, Project administration, Funding acquisition, Conceptualization. **Thomas E. Schellin:** Writing – review & editing, Supervision.

Declaration of competing interest

The authors declare that they have no known competing financial interests or personal relationships that could have appeared to influence the work reported in this paper.

Acknowledgements

This study was funded by the Federal Ministry for Economic Affairs and Energy (BMWi) under grant No. 03SX509B.

Appendix A. Supplementary data

Supplementary data to this article can be found online at https://doi.org/10.1016/j.oceaneng.2024.118648.

References

Akyıldız, H., Ünal, N.E., Aksoy, H., 2013. An experimental investigation of the effects of the ring baffles on liquid sloshing in a rigid cylindrical tank. Ocean. Eng. 59, 190–197.
Bellezi, C.A., Cheng, L.Y., Nishimoto, K., 2022. A numerical study on sloshing mitigation by vertical floating rigid baffle. J. Fluid Struct. 109, 103456.
Cao, Z., Xue, M.A., Yuan, X., Zheng, J., 2023. A fast semi-analytic solution of liquid sloshing in a 2-D tank with dual elastic vertical baffles and walls. Ocean. Eng. 273, 113951.
Cho, J.R., Lee, H.W., 2004. Numerical study on liquid sloshing in baffled tank by nonlinear finite element method. Comput. Methods Appl. Mech. Eng. 193 (23–26), 2581–2598.
Eswaran, M., Saha, U.K., Maity, D., 2009. Effect of baffles on a partially filled cubic tank: numerical simulation and experimental validation. Comput. Struct. 87 (3–4), 198–205.
Gedikli, A., Ergüven, M.E., 1999. Seismic analysis of a liquid storage tank with a baffle. J. Sound Vib. 223 (1), 141–155.
George, A., Cho, I.H., 2021. Anti-slosh effect of a horizontal porous baffle in a swaying/rolling rectangular tank: analytical and experimental approaches. Int. J. Nav. Archit. Ocean Eng. 13, 833–847.
Hasheminejad, S.M., Aghabeigi, M., 2012. Sloshing characteristics in half-full horizontal elliptical tanks with vertical baffles. Appl. Math. Model. 36 (1), 57–71.
Hirt, C.W., Nichols, B.D., 1981. Volume of fluid (VOF) method for the dynamics of free boundaries. Journal of computational physics 39 (1), 201–225.
Jin, X., Liu, M., Zhang, F., Li, D., 2022a. Mitigation of liquid sloshing by multiple layers of dual horizontal baffles with equal/unequal baffle widths. Ocean. Eng. 263, 112184.
Jin, X., Zheng, H., Liu, M., Zhang, F., Yang, Y., Ren, L., 2022b. Damping effects of dual vertical baffles on coupled surge-pitch sloshing in three-dimensional tanks: a numerical investigation. Ocean. Eng. 261, 112130.
Kim, Y., Son, S., Jung, T., Gallien, T., 2021. An analytical and numerical study of a vertically discretized multi-paddle wavemaker for generating free surface and internal waves. Coast. Eng. 165, 103840.
Koh, C.G., Luo, M., Gao, M., Bai, W., 2013. Modelling of liquid sloshing with constrained floating baffle. Comput. Struct. 122, 270–279.
Korkmaz, F.C., 2022. Damping of sloshing impact on bottom-layer fluid by adding a viscous top-layer fluid. Ocean. Eng. 254, 111357.
Liu, D., Lin, P., 2009. Three-dimensional liquid sloshing in a tank with baffles. Ocean. Eng. 36 (2), 202–212.
Maleki, A., Ziyaeifar, M., 2007. Damping enhancement of seismic isolated cylindrical liquid storage tanks using baffles. Eng. Struct. 29 (12), 3227–3240.
Maleki, A., Ziyaeifar, M., 2008. Sloshing damping in cylindrical liquid storage tanks with baffles. J. Sound Vib. 311 (1–2), 372–385.
Menter, F.R., Kuntz, M., Langtry, R., 2003. Ten years of industrial experience with the SST turbulence model. Turbulence, heat and mass transfer 4 (1), 625–632.
Nimisha, P., Jayalekshmi, B.R., Venkataramana, K., 2022. Effective configuration of perforated baffle plate for efficient slosh damping in liquid retaining tanks under lateral excitation. Ocean. Eng. 259, 111855.
Panigrahy, P.K., Saha, U.K., Maity, D., 2009. Experimental studies on sloshing behavior due to horizontal movement of liquids in baffled tanks. Ocean. Eng. 36 (3–4), 213–222.
Park, J., Cho, D., Jang, T., 2023. A numerical experiment on a new piston-type wavemaker: shallow water approximation. Int. J. Nav. Archit. Ocean Eng. 15, 100535.
Prasad, D.D., Ahmed, M.R., Lee, Y.H., Sharma, R.N., 2017. Validation of a piston type wave-maker using Numerical Wave Tank. Ocean. Eng. 131, 57–67.
Qi, Y., Söding, H., el Moctar, O., Neugebauer, J., Schellin, T., 2024. A three-dimensional fully linear finite difference approach to predict waves in tanks excited by ship motions. Ocean. Eng. 302, 117391.
Saghi, R., Ning, D., Mayon, R., Zhao, M., 2022. Evaluation of angular and linear spring systems linked to a dual baffle against the sloshing phenomenon. Ocean. Eng. 266, 113045.
Schäffer, H.A., 1996. Second-order wavemaker theory for irregular waves. Ocean. Eng. 23 (1), 47–88.
Skourup, J., 1996. Active absorption in a numerical wave tank. In: ISOPE International Ocean and Polar Engineering Conference. ISOPE. ISOPE-I).
Skourup, J., Schäffer, H.A., 1997. Wave generation and active absorption in a numerical wave flume. In: ISOPE International Ocean and Polar Engineering Conference. ISOPE-I). ISOPE.
Sun, B., Li, C., Yang, S., Zhang, H., 2021. A simplified method and numerical simulation for wedge-shaped plunger wavemaker. Ocean. Eng. 241, 110023.
Waldie, B., White, G., 2000. Damping characteristics of baffles for suppression of marine motion effects in primary separators. Chem. Eng. Res. Des. 78 (5), 698–706.

Wang, B., Xu, T.J., Jiang, Z.Q., Wang, S., Dong, G.H., Wang, T.Y., 2022. Numerical simulation of sloshing flow in a 2D rectangular tank with porous baffles. Ocean. Eng. 256, 111384.
Wang, J., Gao, J., Sun, Y., 2023. Semi-analytical method for liquid sloshing in the rigid super-elliptical tank with the ring baffle. Ocean. Eng. 281, 114718.
Wu, N.J., Hsiao, S.C., Chen, H.H., Yang, R.Y., 2016. The study on solitary waves generated by a piston-type wave maker. Ocean. Eng. 117, 114–129.
Wu, N.J., Tsay, T.K., Chen, Y.Y., 2014. Generation of stable solitary waves by a piston-type wave maker. Wave Motion 51 (2), 240–255.
Zhang, Z.L., Khalid, M.S.U., Long, T., Chang, J.Z., Liu, M.B., 2020. Investigations on sloshing mitigation using elastic baffles by coupling smoothed finite element method and decoupled finite particle method. J. Fluid Struct. 94, 102942.
Zhou, B.Z., Ning, D.Z., Teng, B., Liu, S.X., 2010. Analytical study on wave making in a deep wave flume in step-type. Wave Motion 47 (1), 1–11.